ADVANCED MATERIALS INTERFACES
Open Access
www.advmatinterfaces.de

Investigating Adsorption of Cellulose Nanocrystals at Air–Liquid and Substrate–Liquid Interfaces after pH Manipulation

*Geosmin A. Turpin, Andrew Nelson, Stephen A. Holt, Luke W. Giles, Izabela Milogrodzka, Roger G. Horn, Rico F. Tabor, and Leonie van't Hag**

Coatings of anisotropic nanoparticles such as cellulose nanocrystals (CNCs) can provide tuneable physicochemical surface properties to a substrate such as modifying wettability. These coatings are often formed using dip coating, with CNCs enriched at the air–water interface transferred to a substrate as a monolayer. This process is commonly facilitated by surfactants, which can remain present in the final product, affecting coating properties. In this work, an "additive free" method for creating CNC coatings by exploiting electrostatic interactions within the pH window between pH 2–4 is demonstrated. Within this pH window, the air–water interface is positively charged and CNCs are negatively charged, with surface pressure tensiometry, X-ray reflectivity, and Brewster angle microscopy indicating that CNCs are driven to the air–water interface. The optimal condition for monolayer coverage was pH 3; at pH 2 charge screening causes localized flocculation at the air–water interface, and at pH 4 interparticle repulsion leads to incomplete, patchy coverage. These findings successfully translate to dip coated CNC monolayers as characterized by atomic force microscopy, showing that the manipulation of pH can facilitate the surfactant-free dip coating of CNCs, with advantages over the surfactants that are more typically used.

1. Introduction

Cellulose nanocrystals (CNCs) are highly negatively charged chemically and physically anisotropic nanoparticles that can be sourced renewably. Their physicochemical properties can be conferred onto substrates by forming coatings, allowing them to be used for many applications such as superhydrophobic coatings for self-cleaning,[1] antifouling and antibacterial properties,[2] improving the printing resolution of paper,[3] or sensing toxic vapors.[4] When coatings are formed by dip coating or Langmuir–Blodgett (LB) deposition, their properties are affected by the behavior of CNCs at both the air–liquid and substrate–liquid interfaces. Normally surfactants are used to facilitate the enrichment of CNCs to the air–liquid interface.[5] This modifies the surface charge of CNCs as well as rendering them more hydrophobic.[6] CNCs and surfactants will form different self-assemblies based on what surfactant is present,[7] and the properties of these self-assemblies can affect how the CNCs align and assemble at the interface in response to compression.[8] This self-assembly behavior impacts the properties of the final coatings, such as the wetting contact angle of CNCs with surfactants present being higher than pure spin-coated CNCs,[9] indicating a difference in surface energy due to the presence of hydrophobic tail groups. There are also routes for covalent modification of CNCs to modify these properties, such as the commonly used 2,2,6,6-tetramethylpiperidine-1-oxyl radical (TEMPO)-mediated conversion of hydroxymethyl groups to carboxylates[10] to make their surface charge more negative,[11] however to our knowledge these modifications are not used to facilitate enrichment of CNCs to the air–liquid interface.

The ORCID identification number(s) for the author(s) of this article can be found under https://doi.org/10.1002/admi.202202452.

[+]Present address: School of Chemistry and the University of Sydney Nano Institute, The University of Sydney, Sydney, New South Wales 2006, Australia

[++]Present address: School of Materials Science and Engineering, UNSW Sydney, Sydney, New South Wales 2052, Australia

DOI: 10.1002/admi.202202452

G. A. Turpin,[+] L. W. Giles,[++] R. G. Horn, R. F. Tabor
School of Chemistry
Monash University
Clayton 3800, Australia

A. Nelson, S. A. Holt
Australian Nuclear Science and Technology Organisation
Lucas Heights, New South Wales 2234, Australia

I. Milogrodzka, L. van't Hag
Department of Chemical and Biological Engineering
Monash University
Clayton 3800, Australia
E-mail: leonie.vanthag@monash.edu

Because CNC is a biologically derived material, it is important to note that different sources and treatments can affect CNC properties such as structure and surface charge, affecting behavior both in the bulk dispersion and at interfaces.[12] This means any comparison of the interfacial behavior of CNCs from different publications must be undertaken carefully if CNCs have been sourced or treated differently. This is important to consider when examining other findings indicating that CNCs can spontaneously adsorb to the air-water interface without surfactants.[13] Although this process is thermodynamically possible, the kinetics of this mechanism make it untenable for coating applications, as the process occurs over the timescale of hours. The addition of salt has been shown to speed this up by driving the formation of CNC aggregates that move more quickly to the air–water interface, however, this is still slower than what can be achieved with surfactants.[13] The addition of salt can also affect the phase of bulk CNCs as well as affect interfacial adsorption and behavior,[14] meaning that such approaches should be undertaken cautiously if pristine coatings are desired. This motivates a deeper effort at understanding the interfacial behavior of CNCs to allow for finer control of both interfacial and bulk properties.

Fundamental studies of spherical nanoparticles have been performed to explore the relationship between the parameters of bulk dispersions and behavior at the air–water interfaces or final coatings. The anisotropic nature and biological sourcing of CNCs can make it difficult to perform direct comparisons to these fundamental studies, especially as geometry,[15] anisotropy,[16] size and concentration[17] can all influence interfacial adsorption. Nonetheless, these fundamental studies provide a useful starting point for considering the complex balance of forces affecting adsorption and coating behaviors.

1.1. Modifying Interfacial Adsorption by pH Manipulation

In a study of 50 nm polystyrene beads, ionic strength has been shown to alter the balances of particle–particle and particle–substrate interactions, affecting the final structure of nanoparticle coatings at and beyond the microscale.[18] More specifically relevant for this work, increasing pH level has been shown to affect nanoparticle deposition, with the energy barrier for particle–substrate attachment increasing more than the energy barrier of particle–particle attachment.[19] There appears to be an optimal pH condition where electrostatic, van der Waals, hydrophilic and hydrophobic forces are ideally balanced for successful coating, beyond which particle–particle interactions dominate too strongly for monolayers to form. Other work has shown that the interfacial adsorption of 4-mercaptobenzoic acid capped gold isotropic spherical nanoparticles with a diameter less than 16 nm can be reversibly controlled through pH manipulation,[20] although these are much smaller than anisotropic CNCs which have typical dimensions of 4–70 nm in width and 100–600 nm in length.[21]

This work is motivated by these previous findings, along with the observation that CNCs stay negatively charged over a wide pH range,[22] and other findings showing the air–water interface is positively charged below pH 4.[23] In particular, we explore whether pH adjustment can provide an optimal condition for coating with the more complicated and anisotropic CNC particles. Our results point to a new, "additive-free" method for enriching CNCs to the air–water interface, with the behavior of these systems in response to compression and changes to pH being used to form a more developed understanding of this new enrichment mechanism. This knowledge was subsequently used to determine the optimal conditions for preparing CNC monolayer coatings on solid substrates through the manipulation of pH alone. Through these investigations, the potential of pH manipulation to facilitate the dip coating of CNCs is demonstrated, as well as provoking investigation into other applications involving surface-based phenomena.

2. Results and Discussion

2.1. CNCs Can Be Enriched to the Air–Water Interface through Charge Manipulation

Cellulose nanocrystals were found to have a negative zeta potential between pH 2 and 5 (**Figure 1**), consistent with previous literature.[22] We also observed a maximum at pH 3.5, consistent with the overlap of the pK_as of functional groups present on CNCs, with sulfate half esters having a pK_a of ≈1.9[24] and the carboxylic groups having a pK_a of 4.5.[25] Below pH 4, the air–water interface has been shown to have a positive surface potential[23,26,27] meaning there is a pH window where CNCs and the air–water interface have surface charges of opposite sign. Surface pressure tensiometry was used to investigate the hypothesis that CNCs are electrostatically driven to enrich to the air–water interface within this pH window.

Surface pressure responses arise from material adsorbed to the air–water interface resisting compression of the interface, either experiencing a deformation or experiencing interparticle repulsion. In this case the surface pressure response confirms that CNCs do enrich to the interface in this pH window (**Figure 2**), when CNCs at a neutral pH show negligible surface pressure and no interfacial enrichment. Both pH 3 and 4 demonstrate strong surface pressure responses, with pH 4 demonstrating a compression response at an earlier onset, indicating

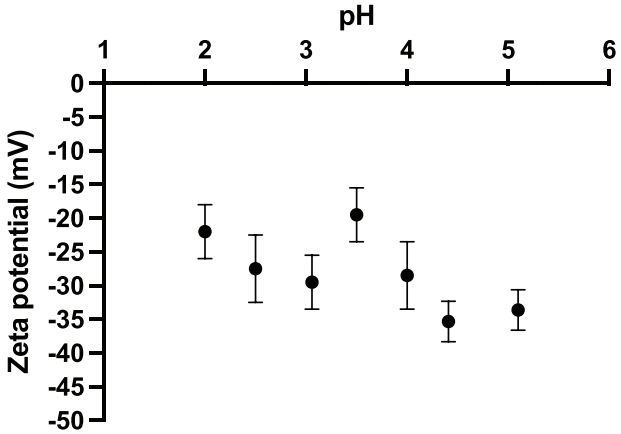

Figure 1. Zeta potential of 0.5 mg mL^{-1} CNC at different pH levels. Vertical error bars represent the standard deviation of the measurements (n = 5).

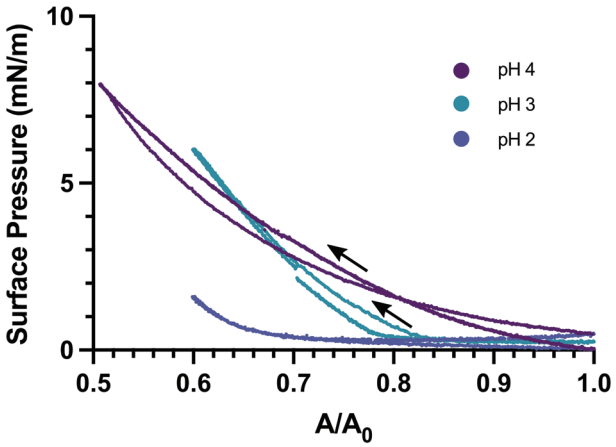

Figure 2. Surface pressure plots obtained for 0.5 mg mL^{-1} aqueous CNC dispersions in air at pH 2, 3, and 4, using Wilhelmy plate tensiometry measured in a Langmuir–Blodgett configuration. Arrows indicate direction of compression. Sample size of presented data for each system and compression level was (n = 1), although trends were consistent across repeated experiments.

longer-range interactions between particles, and pH 3 showing a steeper gradient once the greater amount of compression required is achieved, indicating stronger particle–particle interaction once they do sense each other. These observations can be explained by differences in the Debye length. At pH 4, CNCs experience a ≈3 times stronger interparticle repulsion force upon compression due to ionic strength being 10× weaker than at pH 3, whereas the shorter Debye length of CNCs at pH 3 would cause the stronger interparticle repulsion response observed. It is hypothesized that pH 3 or 2 would have more CNCs enriched to the air–water interface than pH 4 due to greater magnitude in charge difference between CNCs and the interface itself, and this may also explain the stronger compression response observed for pH 3.

Given this reasoning, the system at pH 2 may have the most material enriched at the interface, and yet it demonstrates the weakest surface pressure response. We hypothesize this is due to localized flocculation at the interface, discussed in more detail in the next subsection. The contribution of the potential on the unoccupied air–water interface is relatively small for particles much larger than their Debye length,[28] however at pH 2 the Debye length is expected to be too short for CNCs to remain stably adsorbed at the air–water interface at that pH, with van der Waals forces dominating, causing flocculation and reducing any surface pressure response mostly to physical deformation of the flocs, with little contribution from electrical double layer repulsion. This is supported by previous findings showing that increasing ionic strength can cause network structures to form between CNCs,[14] with pH 2 being the flocculation threshold for CNCs.[29]

Interestingly, when this behavior was checked via dynamic light scattering (DLS), all samples showed a diameter of 100 nm ± 5 nm (Figure S1, Supporting Information), the same as CNCs at a native pH of 6. This contrasts with previous papers suggesting that the targeted addition of salt accelerates the enrichment of CNCs to the air–water interface by first driving the aggregation of CNCs,[30] as our findings indicate that flocculation is not occurring in the bulk, but instead is localized entirely to the air–water interface. Other findings from the same group do indicate a structural change at the air–water interface in response to changes in ionic strength, as demonstrated through changes in interfacial viscoelasticity.[13] These discrepancies may be because changing pH influences not only the ionic strength of the aqueous medium but also the zeta potential of the nanoparticles and the surface potential of the air–water interface, prompting X-ray reflectivity (XRR) experiments to elucidate the air–water interfacial adsorption behavior of CNCs in response to the manipulation of pH and interfacial compression.

2.2. Compression and pH Affect how CNCs Arrange at the Air–Water Interface

XRR measurements were performed on 0.5 mg mL^{-1} dispersions of CNCs in a Langmuir trough at pH 2, 3, and 4 at compressions from A/A_0 = 1.0 (uncompressed) to A/A_0 = 0.3 (compressed to 30% of original area) (Figure S3, Supporting Information). The reflectivity profiles for all pH levels and compressions could be fit with a single layer that possessed the thickness (≈4 nm) and scattering length density (SLD) of cellulose nanocrystals (Tables S1–S3, Supporting Information), confirming the presence of CNCs at the air–water interface. When comparing the reflectivity profiles between systems with differing pH and compression, no significant distinction could be made due to the large margins of uncertainty arising from the required fitting process. This is notable when considering the flocs hypothesized to form at pH 2, indicating they may be on a size scale different to what is observable using XRR. This motivates the use of Brewster angle microscopy (BAM) as a complementary technique to directly image the CNCs and any changes to their microscale interfacial assembly behavior.

BAM was successfully used to directly image CNCs adsorbed at the air–water interface in order to better assess the impact pH has on the adsorption behavior of CNCs as a function of compression (**Figure 3**). At pH 2, we can visually confirm the hypothesis of interfacially-confined flocculation occurring even for uncompressed interfaces. This supports our interpretations of surface pressure tensiometry, although it is interesting to note the significant compression response in the BAM images given the relatively weak surface pressure response. At pH 3, we see relatively homogeneous features, with the brightness indicating an adsorbed layer that should be a monolayer according to XRR measurements. What starts as fairly consistent coverage gets more patchy as compression occurs. Features were more difficult to observe for pH 4, with individual patches or islands supporting the hypothesis of less complete coverage.

At the highest compression condition, all interfaces showed patchy coverage and the emergence of circular self-assemblies. These may be related to circular domains previously observed during BAM of CNC and dioctadecyldimethylammonium systems,[31] however the presence of surfactant and the different size scales of the BAM may limit how instructive this comparison is. The main wisdom we can extract from these findings is that CNCs do adsorb best to the air–water interface at pH 3, and that less compressed interfaces seem more favorable for

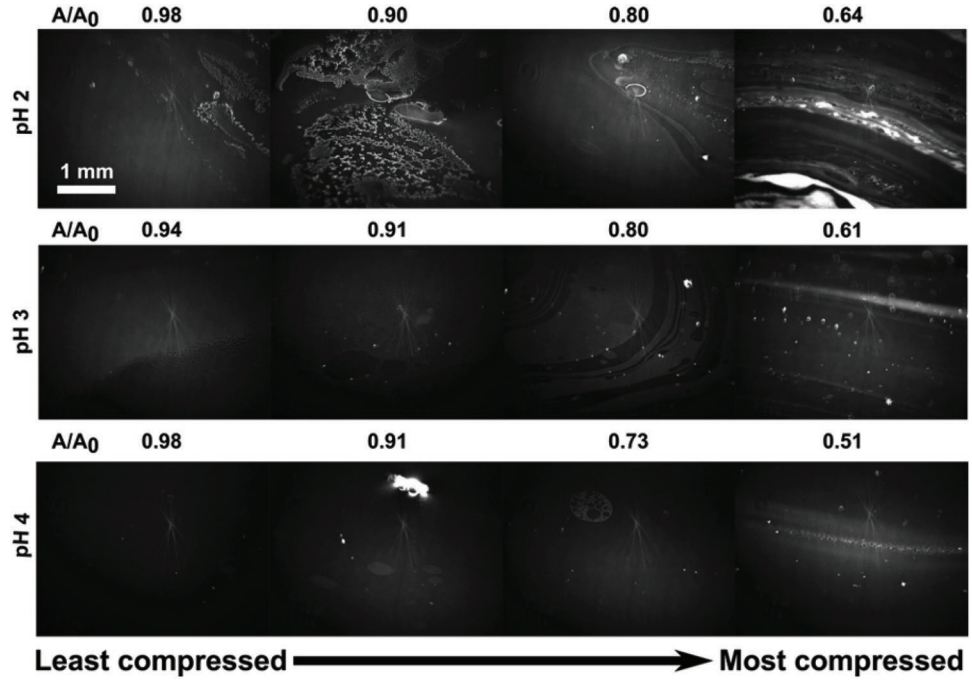

Figure 3. Brewster angle microscopy images of 0.5 mg mL^{-1} CNC at pH 2, 3, and 4 at different extents of interfacial compression. Scale bar equal to 1 mm, with the same field of view for all images. Arrow indicates progression of compression with the leftmost figures being least compressed, and rightmost figures being most compressed. The star-like feature (most prominently visible at pH 3, $A/A_0 = 0.98$, but present in all images) is a visual artefact and should not be interpreted as material adsorbed to the interface. Sample size of presented data for each system and compression level was ($n = 1$), although trends were consistent across repeated experiments.

dip coating. As surfactant-free CNC dip coating processes have been previously demonstrated to have a significant contribution of adsorption from the bulk dispersion at the substrate–liquid interface as well as from CNCs interfacially enriched to the air–liquid interface,[9] this motivates an investigation into how adsorption from the bulk contributes in this process and how this changes with pH, even if we hypothesize that the process is dominated by air–water interface interactions.

2.3. Assessing the Contribution of Bulk Adsorption Processes

Force measurements using atomic force microscopy (AFM) were undertaken on clean glass substrates submerged in aqueous dispersions of 0.5 mg mL^{-1} CNCs at pH 2, 3, and 4 to assess whether there were any contributions from bulk adsorption to the coating process, and how these may change with pH (**Figure 4**a). At all pH levels, there is a visible force response starting around ≈40 nm, with the consistency of this position suggesting this is more likely to be due to the tip encountering actual, physically adsorbed material at the interface rather than repulsive forces as it is still consistent when ionic strength is greatly varying. This suggests that there is some contribution of adsorption from the bulk when dip coating these systems, although assessing the magnitude of this contribution becomes challenging.

At pH 4, there is a distinctly observable breakthrough at approximately 4 nm from the glass surface (Figure 4a,b), with this dimension consistent with a single monolayer of CNCs adsorbed to silica as previously determined using quartz crystal microbalance measurements,[9] as well as the dimensions of the adsorbed layer measured at the air–water interface via XRR (Table S3, Supporting Information). This potentially indicates the presence of an adsorbed monolayer from the bulk dispersion at this pH level. The weak breakthrough force required indicates that the layer is easily disrupted (Figure 4c), requiring approximately 30 times less force than what is required to break a lipid bilayer at the same temperature and ionic strength.[32] These rearrangement or breakthrough events are less distinct at pH 2 and 3, meaning the dimensions of any closely-adsorbed CNC layers, or the breakthrough strengths required to disrupt them cannot be directly compared, however, the different shapes of the force curves could correspond to a changing balance of particle–particle and particle–substrate interactions, as particle–substrate interactions have previously been shown to become less dominant with increasing pH.[18]

Given that we are confident that pH manipulation can facilitate the adsorption of CNCs to the air–water interface and there appears to be a contribution from adsorption from the bulk dispersion as well, we should be able to exploit our findings in order to form surfactant-free monolayer coatings of cellulose nanocrystals through dip coating using pH manipulation alone.

2.4. Manipulation of pH Can Be Exploited to Form Additive-Free CNC Monolayer Coatings

Using AFM to image plasma-cleaned glass slides that were dip coated into aqueous CNC dispersions at different pH levels supports our hypotheses and interpretations of our BAM images

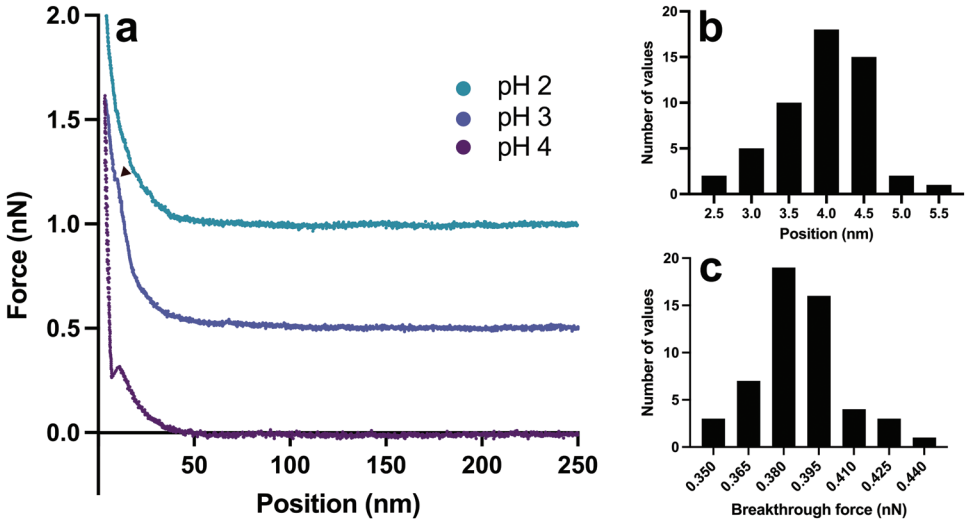

Figure 4. a) Overlaid AFM-force profiles obtained on a cleaned glass substrate in aqueous dispersions of 0.5 mg mL^{-1} CNCs at pH 2, 3, and 4. Data for pH 3 and pH 2 has been offset by + 0.5 and + 1.0 nN, respectively. Force curve for pH 4 was measured at 1 µm s^{-1}, and pH 2 and 3 were measured at 0.5 µm s^{-1}. b) Frequency distribution of the breakthrough position for CNC layer adsorbed to glass substrate at pH 4 ($n = 64$). c) Frequency distribution of force required to break through adsorbed CNC layer at pH 4 ($n = 64$).

(**Figure 5**). CNCs at pH 3 demonstrate an "additive-free" method for forming a monolayer coating, consistent with tensiometry, XRR, and BAM results. At pH 4, patchier coverage can be observed with CNCs drying in islands, consistent with previous fundamental studies showing how increasing pH level changes nanoparticle deposition patterns, as the energy barrier of particle–substrate attachment demonstrates a greater increase than that of particle–particle attachment.[19] The interfacial

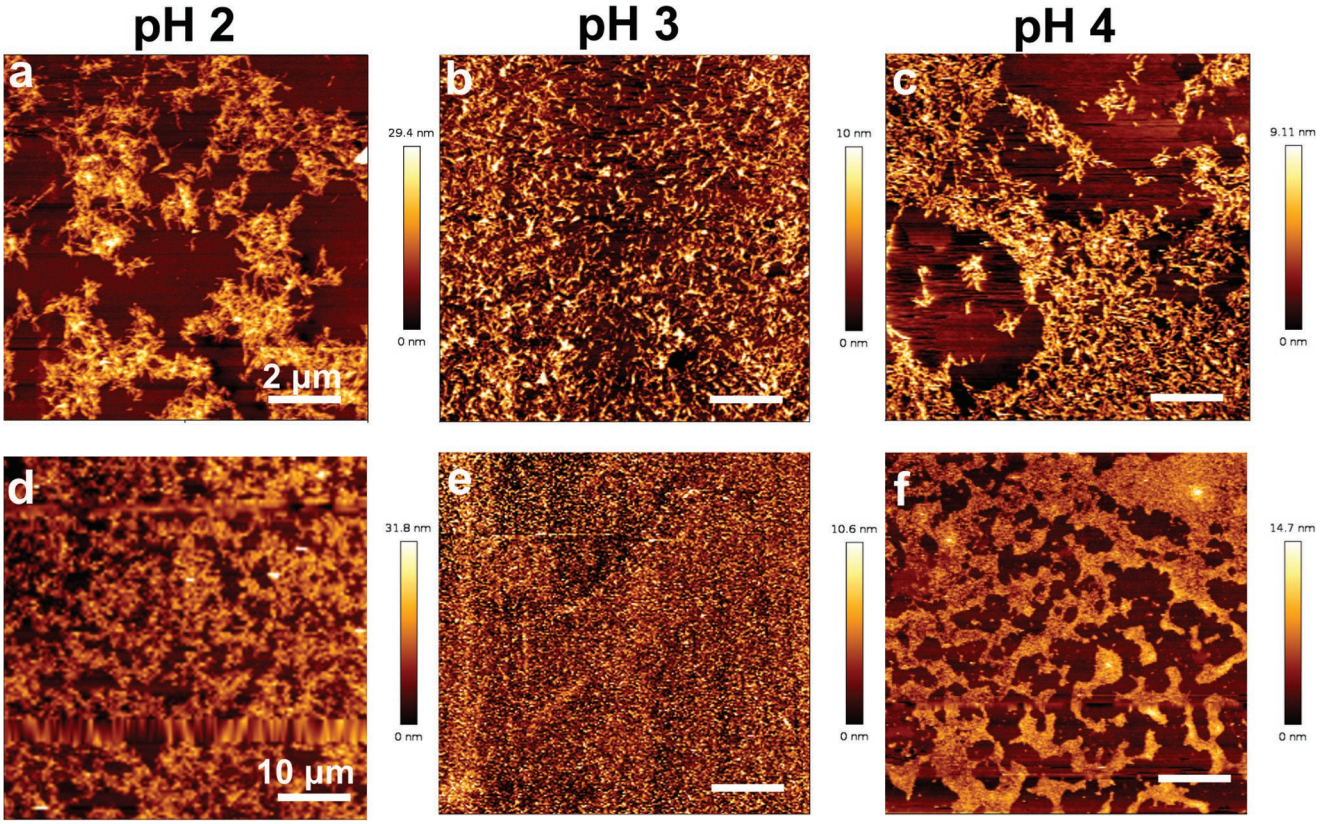

Figure 5. Atomic force microscope images of CNCs on plasma-cleaned hydrophilic glass substrate, prepared by manually dip-coating from 0.5 mg mL^{-1} aqueous CNC dispersions at different pH levels. a–c) Coating prepared at pH 2.0, 3.0, and 4.0, respectively, scale bar = 2 µm. d–f) Same coatings with a wider field of view, scale bar = 10 µm.

ADVANCED MATERIALS INTERFACES
Open Access
www.advmatinterfaces.de

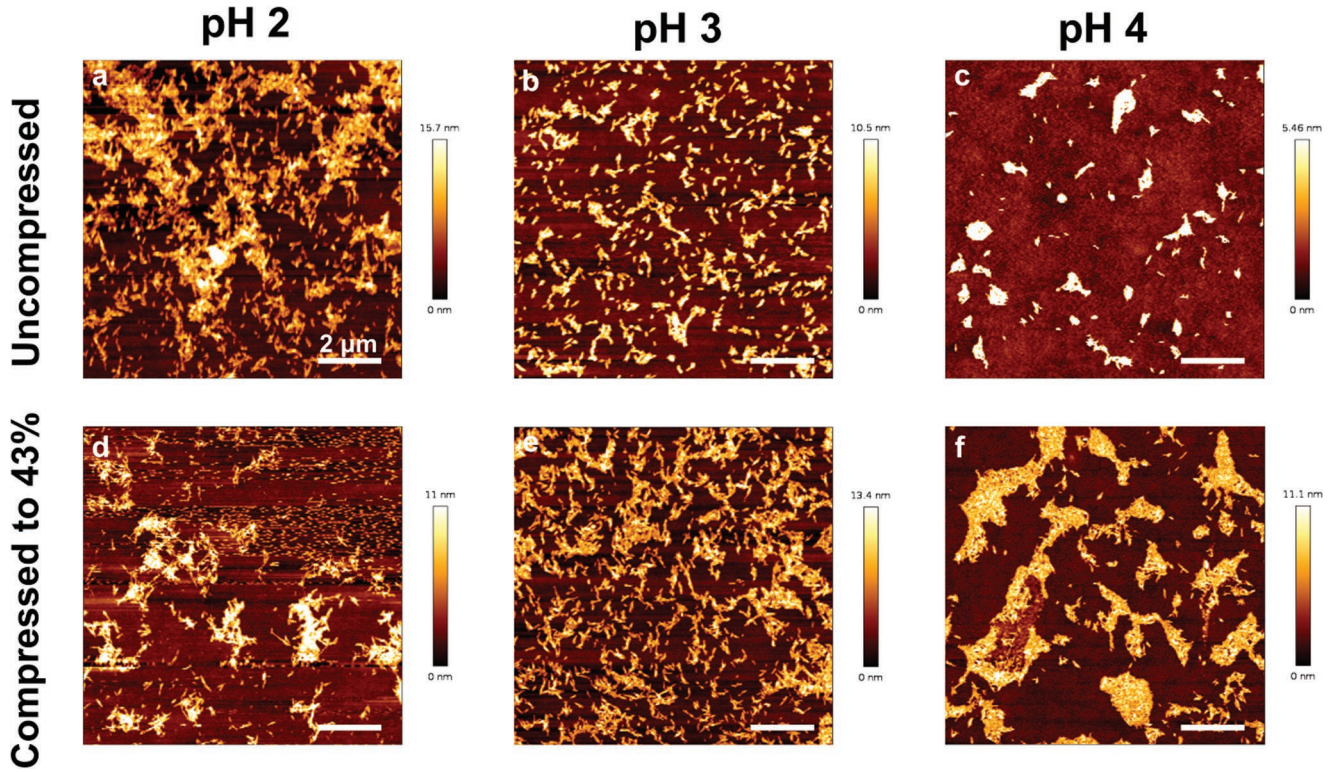

Figure 6. Atomic force microscope images of CNCs on plasma-cleaned hydrophilic glass substrate, prepared by Langmuir–Blodgett deposition from 0.5 mg mL^{-1} aqueous CNC dispersions at different pH levels. a–c) Coatings prepared from an uncompressed interface at pH 2.0, 3.0, and 4.0, respectively. d–f) Coatings prepared from an interface compressed to $A/A_0 = 0.43$ at pH 2.0, 3.0, and 4.0, respectively. Scale bar = 2 µm for all images.

flocculation visible for the coating at pH 2 is consistent with Debye length being short enough to allow for strong particle–particle interactions. It is also important to consider interactions between particle and substrate, as the zeta potential of glass surfaces has also been shown to decrease by at least 10 mV in the window between pH 2 and pH 4.[35] Furthermore, consideration of the effect of ionic strength on the delicate balance of these forces is essential if these coating methods are to be scaled up, as effects on nanoscale arrangement have been shown to affect arrangement beyond the microscale.[18]

These coatings resulted from manually dip coating an uncompressed interface, as findings from both XRR and BAM indicated that compression caused unfavorable disturbances at the air–water interface. We attempted to confirm the impact of interfacial compression by repeating these experiments using Langmuir–Blodgett deposition to allow us to compress the interface. Although the same general outcomes were consistent, with pH 2 flocculating, pH 3 showing the best coverage, and pH 4 showing islands of CNCs, the resultant coatings were patchier than those formed using manual deposition (**Figure 6**). As this occurred for both compressed and uncompressed systems, we interpret this as being due to the slower dipping process required for LB deposition causing a different drying mechanism to the faster manual dip coating process, as the drying mechanism can have a large impact on self-assembly behavior during deposition,[18,36] with careful modification of this parameter potentially allowing for finer control of these coating processes in the future.

Interestingly, it does appear that interfacial compression can subtly affect the texture of the final coatings, and we have not seen a compression response in similar previous experiments with CNCs and hydrotropes, supporting the hypothesis that this pH-controlled, electrostatically driven mechanism of enrichment is different from the manipulation of amphiphilicity imbued by hydrotropes.[9] This sensitivity to compression suggests that although it is likely that adsorption from the bulk does occur, it is the pH-controlled enrichment of CNCs to the air–water interface that dominates this coating mechanism, being exploited in order to form surfactant-free monolayer coatings. The ideal conditions for forming a monolayer in this system are a 0.5 mg mL^{-1} CNC dispersion at pH 3, an uncompressed interface, and a relatively quick dip coating method. These findings provoke more fundamental investigations into whether this electrostatically driven, pH-manipulated "additive-free" interfacial enrichment process can be repeated to form monolayer coatings of other anisotropic nanoparticles in the future, circumventing the complications these additives can introduce as well as providing further fundamental insight into the adsorption behavior of nanoparticles at interfaces.

3. Conclusion

By studying adsorption behavior at both air–water and substrate–water interfaces, we have developed an "additive-free"

method of enriching CNCs to the interface through manipulating charge. This works because of the pH window between 2 and 4, where the air–water interface is positively charged and CNCs are negatively charged. At pH 4, there is too much interparticle repulsion for monolayer coverage, and at pH 2, there is too much localized interfacial flocculation, whereas pH 3 was found to be optimal for monolayer coverage. These optimal conditions translated to monolayer coatings formed after dip coating. The process seems to be dominated by the enrichment of CNCs at the air–water interface, with some potential contribution from interactions between the substrate and bulk dispersion. This work highlights how fundamental studies into the adsorption behavior of nanoparticles at both substrate–water and air–water interfaces can provide a fundamental understanding of the competing coating processes herein, resulting in a finer control of desired coating properties after dip coating and a resultant surfactant-free coating monolayer of anisotropic nanoparticles. As this monolayer enrichment could be achieved through the manipulation of pH alone, expanding this investigation into the substrate–water and air–water adsorption behavior of other anisotropic nanoparticle systems with a pH window where there is a charge difference between particle and interface would likely prove fruitful for a better understanding of these surfactant-free coating techniques. This will hopefully have future applications in systems where dip coating is necessary, but some properties contributed by surfactants are not welcome.

4. Experimental Section

Materials: Cellulose nanocrystals were purchased from the University of Maine Process Development Centre (11.5–12.5% aqueous gel, 0.85% sulfonation). HCl used for pH correction was purchased from Sigma and used without further purification. All dispersions/solutions were made up with ultra pure water dispensed from a Millipore Direct-Q 5 system.

Particle Sizing and Zeta Potential Measurements: Measurements were performed on a Brookhaven Nanobrook Omni instrument. Particle sizing experiments were performed using DLS, with each measurement involving three runs of five cycles at 25 °C. Zeta potential measurements were performed using phase analysis light scattering on a Brookhaven Nanobrook Omni instrument. Each measurement involved five consecutive runs comprising 20 cycles at 25 °C. Samples were 0.5 mg mL^{-1} dispersions of CNCs in the presence of listed salts.

X-Ray Reflectivity and Langmuir Trough Surface Pressure Tensiometry: Specular XRR measurements of the air–liquid interface were performed using a PANanalytical X-Pert PRO reflectometer (high tension = 45 kV, current = 40 mA) with a radiation wavelength (Cu $K\alpha$) of 0.15418 nm. Measurements were 60 min in duration, covering a q-range of ≈0.01 to 0.4 $Å^{-1}$. Samples were contained in a PTFE Langmuir trough (7 cm × 15 cm, Nima Technology Ltd.) and sealed in a closed environment to minimize evaporation. The reflectometer enclosure temperature was ≈26 °C. All reflectivity data was modeled using Refnx, a python-based reflectivity analysis software package[37,38] after cutting the Q range to between 0.06 and 0.25 to avoid issues with overfitting the critical edge. Surface pressure was measured with the same Langmuir trough, using a Wilhelmy plate (2.35 × 1 cm^2, Whatman CHR1 filter paper) attached to a pressure sensor. Surface pressure-area isotherms for these systems were performed with a barrier speed of 36 mm min^{-1}.

Langmuir–Blodgett Deposition: Dip coating was performed on glass slide substrates washed with acetone, ethanol, and ultra pure water before being plasma cleaned in an air plasma (Model PDC 002, Harrick Scientific Corporation) and treated with 30 W plasma power for 7 min. The trough was washed with Hellmanex, ethanol and ultra pure water before being wiped with a Kimwipe and washed with ultra pure water again, with this cycle being repeated until measured surface pressure was below 0.3 mN m^{-1} at full compression. Surface pressure was measured with the same Langmuir trough, using a Wilhelmy plate (2.35 × 1 cm^2, Whatman CHR1 filter paper) attached to a pressure sensor. Surface pressure-area isotherms for these systems were performed at a rate of 36 mm min^{-1}. The coating dispersion was 500 mL of 0.5 mg mL^{-1} CNCs corrected to the desired pH.

Coating was performed with the substrate initially submerged, being inserted in at a rate of 5 mm min^{-1}. Barriers were then closed and opened at a rate of 5 mm min^{-1} in order to achieve desired level of compression. Substrate was kept in the dispersion medium for 15 min before being retracted at a rate of 3 mm min^{-1} in a single pass. Coating process was repeated at two compression points at 100% and 43% of initial interfacial area, with the interface being refreshed and the coating performed on fresh slides each time. Slides were allowed to air-dry before being stored at room temperature in a plastic petri dish.

Manual Dip Coating: Dip coating was performed on glass slide substrates washed with acetone, ethanol, and ultra pure water before being plasma cleaned in an air plasma (Model PDC 002, Harrick Scientific Corporation) and treated with 30 W plasma power for 7 min. Glass slides were manually inserted into vials containing dispersions of 0.5 mg mL^{-1} CNC at pH 2, 3, or 4 at a rate of ≈60 mm min^{-1}. Samples were incubated for 90 s before being removed at a rate of ≈60 mm min^{-1}.

Brewster Angle Microscopy: Brewster angle microscopy images were taken using a KSV NIMA MicroBAM at an angle-of-incidence of 59° with a 50 mW, 659 nm laser emitting p-polarized light, in the same Langmuir trough, with a barrier speed of 5 mm min^{-1}.

Atomic Force Microscopy: Height profiles of dip-coated glass were taken using a JPK Nanowizard 3 in AC (alternating contact mode) in air, with Bruker Model NHCV cantilevers, with nominal resonant frequencies of 340 kHz. Force measurements were measured in liquid using the same instrument. Glass substrates were cleaned using the same method as preparing samples prior to Langmuir–Blodgett deposition, before being submerged in aqueous dispersions of 0.5 mg mL^{-1} CNC previously adjusted to pH 2, 3, and 4. Force measurements being performed after equilibration to assess the adsorption from the bulk dispersion. Measurements were performed using Bruker MSCT cantilevers at an approach velocity of 1 μm s^{-1} for the pH 4 system 0.5 μm s^{-1} for the pH 2 and 3 systems and 64 measurement points. Spring constants for each cantilever were measured using the Bechhoefer and Hutter thermal method.[39]

Statistical Analysis: i) Preprocessing of data: AFM data were processed with a polynomial baseline correction following removal of defect lines (up to 3 per 256 line image). Surface pressure was calculated as the change in surface tension in mN m^{-1} from an uncompressed system, normalized to A/A_0. ii) Data presentation and sample size (n): DLS (three runs of five cycles), zeta potential (five runs of 20 cycles) were presented as mean ± standard deviation. Breakthrough force measurements were presented as frequency histograms with bins of 0.5 nm for distance and 0.015 nN for force (n = 64). Surface pressure was presented in mN m^{-1} as a function of compression (A/A_0) (presented with n = 1, but qualitatively consistent across pendant drop tensiometry experiments and two different Langmuir troughs). XRR data were reduced to 1D intensity versus q plots and presented as the mean ± standard deviation, with corresponding scattering length density profiles (n = 1 for each system at each compression level).

Supporting Information

Supporting Information is available from the Wiley Online Library or from the author.

Acknowledgements

The authors would like to acknowledge the Australian Centre for Neutron Scattering, Australian Nuclear Science and Technology Organisation,

for use of their X-ray reflectivity instrumentation (P9494). This work was supported in part by the grant of an ARC Future Fellowship (FT160100191) to R.F.T. and an Australian Government Research Training Program Scholarship, a Monash Graduate Excellence Scholarship, and a Graduate Research Completion Award to G.A.T.

Open access publishing facilitated by Monash University, as part of the Wiley - Monash University agreement via the Council of Australian University Librarians.

Conflict of Interest

The authors declare no conflict of interest.

Data Availability Statement

The data that support the findings of this study are available from the corresponding author upon reasonable request.

Keywords

adsorption, cellulose nanocrystals, coating, pH manipulation, reflectometry

Received: December 9, 2022
Revised: January 23, 2023
Published online: March 3, 2023

[1] J. Huang, S. Wang, S. Lyu, F. Fu, *Ind. Crops Prod.* **2018**, *122*, 438.
[2] A. Aguilar-Sanchez, B. Jalvo, A. Mautner, S. Nameer, T. Pöhler, T. Tammelin, A. P. Mathew, *J. Membr. Sci.* **2021**, *620*, 118842.
[3] R. Prathapan, B. A. Glatz, A. K. Ghosh, S. Michel, A. Fery, G. Garnier, R. F. Tabor, *Langmuir* **2019**, *35*, 7155.
[4] Y. Zhao, G. Gao, D. Liu, D. Tian, Y. Zhu, Y. Chang, *Carbohydr. Polym.* **2017**, *174*, 39.
[5] Y. Habibi, I. Hoeger, S. S. Kelley, O. J. Rojas, *Langmuir* **2010**, *26*, 990.
[6] Z. Hu, S. Ballinger, R. Pelton, E. D. Cranston, *J. Colloid Interface Sci.* **2015**, *439*, 139.
[7] C. Brinatti, J. Huang, R. M. Berry, K. C. Tam, W. Loh, *Langmuir* **2016**, *32*, 689.
[8] I. Chae, D. Ngo, M. Makarem, Z. Ounaies, S. H. Kim, *J. Phys. Chem. C* **2019**, *123*, 25628.
[9] G. A. Turpin, A. Nelson, S. A. Holt, L. W. Giles, I. Milogrodzka, B. M. Teo, V. S. Raghuwanshi, R. G. Horn, L. van 't Hag, R. F. Tabor, *Adv. Mater. Interfaces* **2022**, *9*, 2200791.
[10] A. De Nooy, A. Besemer, H. Van Bekkum, *Recl. Trav. Chim. Pays-Bas* **1994**, *113*, 165.
[11] Z. Karim, M. Hakalahti, T. Tammelin, A. P. Mathew, *RSC Adv.* **2017**, *7*, 5232.
[12] M. S. Reid, M. Villalobos, E. D. Cranston, *Langmuir* **2017**, *33*, 1583.
[13] P. Bertsch, P. Fischer, *Langmuir* **2019**, *35*, 7937.
[14] Y. Xu, A. D. Atrens, J. R. Stokes, *Soft Matter* **2018**, *14*, 1953.
[15] G. B. Davies, T. Krüger, P. V. Coveney, J. Harting, F. Bresme, *Soft Matter* **2014**, *10*, 6742.
[16] L. Botto, E. P. Lewandowski, M. Cavallaro, K. J. Stebe, *Soft Matter* **2012**, *8*, 9957.
[17] S. Kutuzov, J. He, R. Tangirala, T. Emrick, T. P. Russell, A. Boker, *Phys. Chem. Chem. Phys.* **2007**, *9*, 6351.
[18] E. Homede, A. Zigelman, L. Abezgauz, O. Manor, *J. Phys. Chem. Lett.* **2018**, *9*, 5226.
[19] E. Homede, M. Abo Jabal, O. Manor, *Adv. Funct. Mater.* **2020**, *30*, 2005486.
[20] F. Reincke, W. K. Kegel, H. Zhang, M. Nolte, D. Wang, D. Vanmaekelbergh, H. Möhwald, *Phys. Chem. Chem. Phys.* **2006**, *8*, 3828.
[21] S. Naz, J. S. Ali, M. Zia, *Bio-Des. Manuf.* **2019**, *2*, 187.
[22] R. Prathapan, R. Thapa, G. Garnier, R. F. Tabor, *Colloids Surf., A* **2016**, *509*, 11.
[23] R. F. Tabor, D. Y. Chan, F. Grieser, R. R. Dagastine, *Angew. Chem.* **2011**, *123*, 3516.
[24] D. Klemm, F. Kramer, S. Moritz, T. Lindström, M. Ankerfors, D. Gray, A. Dorris, *Angew. Chem., Int. Ed.* **2011**, *50*, 5438.
[25] A. B. Fall, S. B. Lindström, O. Sundman, L. Ödberg, L. Wågberg, *Langmuir* **2011**, *27*, 11332.
[26] P. Creux, J. Lachaise, A. Graciaa, J. K. Beattie, A. M. Djerdjev, *J. Phys. Chem. B* **2009**, *113*, 14146.
[27] J. K. Beattie, A. M. Djerdjev, G. G. Warr, *Faraday Discuss.* **2009**, *141*, 31.
[28] A. Zigelman, O. Manor, *Langmuir* **2020**, *36*, 4942.
[29] W. Qi, J. Yu, Z. Zhang, H.-N. Xu, *Mater. Res. Express* **2019**, *6*, 125078.
[30] P. Bertsch, M. Diener, J. Adamcik, N. Scheuble, T. Geue, R. Mezzenga, P. Fischer, *Langmuir* **2018**, *34*, 15195.
[31] Y. Habibi, L. Foulon, V. Aguié-Béghin, M. Molinari, R. Douillard, *J. Colloid Interface Sci.* **2007**, *316*, 388.
[32] S. Garcia-Manyes, G. Oncins, F. Sanz, *Biophys. J.* **2005**, *89*, 4261.
[33] F. S. Lameiras, A. L. d. Souza, V. A. R. d. Melo, E. H. M. Nunes, I. D. Braga, *Mater. Res.* **2008**, *11*, 217.
[34] M. Amadu, A. Miadonye, *Int. J. Chem.* **2017**, *9*, 67.
[35] Y. Gu, D. Li, *J. Colloid Interface Sci.* **2000**, *226*, 328.
[36] A. Gençer, C. Schütz, W. Thielemans, *Langmuir* **2017**, *33*, 228.
[37] A. Nelson, *J. Appl. Crystallogr.* **2006**, *39*, 273.
[38] A. R. Nelson, S. W. Prescott, *J. Appl. Crystallogr.* **2019**, *52*, 193.
[39] J. L. Hutter, J. Bechhoefer, *Rev. Sci. Instrum.* **1993**, *64*, 1868.